Applied Surface Science 588 (2022) 152887

Contents lists available at ScienceDirect

Applied Surface Science

journal homepage: www.elsevier.com/locate/apsusc

Full Length Article

Fabrication of novel Z-scheme $LaCoO_3$/activated biochar/Ag_3PO_4 heterojunctions for intensifying visible-light-catalytic degradation of bisphenol A

Xinyan Bu [a], Congjin Chen [a,b,*], Xilian Zhao [a], Quanlong Huang [a], Xiufen Liao [a], Hui Fan [a], Peiwen Wang [a], Huayu Hu [a], Yanjuan Zhang [a], Zuqiang Huang [a]

[a] School of Chemistry and Chemical Engineering, Guangxi University, Nanning 530004, China
[b] Guangxi Key Laboratory of Petrochemical Resource Processing and Process Intensification Technology, School of Chemistry and Chemical Engineering, Guangxi University, Nanning 530004, China

ARTICLE INFO

Keywords:
$LaCoO_3$/AC/Ag_3PO_4composite
Bisphenol A
Z-scheme heterojunctions
Photocatalytic mechanism
Degradation pathway

ABSTRACT

A novel Z-scheme $LaCoO_3$/activated biochar(AC)/Ag_3PO_4 heterojunctions was fabricated and characterized by XRD, SEM-EDS, TEM, XPS, FTIR, N_2 adsorption–desorption isotherms, UV–Vis-DRS, PL and EIS. The catalytic activity of the photocatalyst was investigated via bisphenol A (BPA) photocatalitic degradation. The results showed that the photodegradation efficiencies of BPA catalyzed by $LaCoO_3$/AC/Ag_3PO_4 (2:1:10) composite (reached 99 % after 50 min) was superior to those catalyzed by $LaCoO_3$, Ag_3PO_4, and $LaCoO_3$/Ag_3PO_4 (2:10). The BPA photodegradation followed the pseudo-first-order kinetic model, the photodegradation rate constants *k* catalyzed by $LaCoO_3$/AC/Ag_3PO_4 (2:1:10) was 10.88 times of that catalyzed by Ag_3PO_4, 1.56 times of that catalyzed by $LaCoO_3$/Ag_3PO_4 (2:10). Based on the results of characterization and the experiments of trapping active species in photocatalytic degradation process, the transfer of photo-generated carriers and Z-scheme $LaCoO_3$/AC/Ag_3PO_4 heterojunctions photocatalytic mechanism were proposed. Furthermore, the possible BPA degradation pathways were involved in hydroxylation, oxidation, ketonization and cyclic cleavage. Z-scheme $LaCoO_3$/AC/Ag_3PO_4 heterojunctions can be used as an efficient photocatalyst for practical applications in the removal of endocrine disrupting chemical.

1. Introduction

In recent years, the deterioration of the environment affects people everywhere, especially the water pollution [1,2]. Phenolic compounds are widely used in manufacturing industry and released into the natural water bodies, which is exceedingly harmful to human health [3–5]. Bisphenol A (BPA), as an endocrine disrupting chemical (EDC), has adversely affected the reproductive system, even there are a certain risk of carcinogenicity and teratogenicity to animals and mankind, it must be removed from the polluted water bodies and the other environment [6–8].

Semiconductor-based photocatalysis has been widely regarded as one of the promising, environment-friendly technology to utilize the inexhaustible solar energy to remove and degrade organic pollutants i.e. antibiotics, hazardous dyes or to photocatalyze hydrogen generation [9–14]. Among these semiconductors photocatalysis, the silver-based semiconductors photocatalysis has attracted a plenty of attention. The silver phosphate (Ag_3PO_4) semiconductors photocatalysis, an important silver-based photocatalysis, as one of the efficient photocatalysts, have stimulated increasing interest owing to its remarkable photocatalytic properties [15–18]. However, the practical application of single Ag_3PO_4 photocatalysis has not been achieved to date, because Ag_3PO_4 photocatalyst has inherent photocorrosion defects from the photogenerated electron-hole (e^-–h^+) pairs ($4Ag_3PO_4 + 6H_2O + 12\ h^+ + 12e^- \rightarrow 12Ag + 4H_3PO_4 + 3O_2$) and the rapid recombination of e^-–h^+ pairs, the inherent photocorrosion results in the poor stability of Ag_3PO_4 [18–20]. In order to achieve a high stability, several methodologies are being developed to enhance the photocorrosion resistance and photocatalytic activities of Ag_3PO_4, including morphology control [21,22], combining with other semiconductors to form Z-Scheme heterojunction [23,24], coupling with carbon materials [25–27]. A direct Z-scheme heterojunction could be constructed for changing the transfer path of the photo-generated

* Corresponding author at: School of Chemistry and Chemical Engineering, Guangxi University, Nanning 530004, China.
E-mail address: gxdxccj@163.com (C. Chen).

https://doi.org/10.1016/j.apsusc.2022.152887
Received 21 August 2021; Received in revised form 26 January 2022; Accepted 18 February 2022
Available online 26 February 2022

carriers, promoting light-harvesting ability in the visible-light region. For instance, Shi et al [28] synthesized the $Ag_3PO_4/CuBi_2O_4$ composites, achieving a high stability and photocatalytic efficiency; Liu et al [29] combined Ag_3PO_4 with polyaniline (PNAI) to prepared Ag_3PO_4@PANI composite photocatalyst with a high stability. When graphene/reduced graphene (GO/RGO) was utilized to support Ag_3PO_4, the photogenerated electron conduction became more easily, the recombination rate of e^-–h^+ pairs, the photocorrosion rate of Ag_3PO_4 was both reduced, the photocatalysis efficiency was enhanced, and the photostability of the Ag_3PO_4 composites photocatalysts was improved [30]. Compared to the single Ag_3PO_4 photocatalysts, the higher photostability and faster separation rate of e^-–h^+ pairs of these Ag_3PO_4 composites photocatalysts lead to the photocatalytic performance enhancement [18].

The lanthanum cobaltite ($LaCoO_3$), as a typical perovskite-type transition metal oxide, has been paid extensive attention to degradation of organic pollutants owing to its distinctive crystal structure, superior photoelectrical property, environment-friendly, and low-cost [31,32]. However, the photocatalytic activity of $LaCoO_3$ is restricted owing to speedy recombination of photo-generated electron-hole pairs (e^-–h^+) [33]. Comfortingly, the formed composite photocatalysts via metal or nonmetal ion doping, fabrication method modification and combination with other semiconductors can boost photocatalytic activity compared to single $LaCoO_3$ semiconductor, especially, combining with other semiconductor is a feasible, flexible and effective method to decrease e^-–h^+ recombination and induce photocatalytic efficiency enhancement [33,34].

In order to construct heterojunction photocatalyst with high visible-light catalytic activity, semiconductor materials with a suitable energy band potential that possesses overlaping and staggered conduction band and valence band must be provided. Ag_3PO_4 possesses a narrow band gap (E_g, about 2.40 eV) [18], the conduction band potential of Ag_3PO_4 is 0.45 V [30]. $LaCoO_3$ possesses a band gap of about 0.6 eV for the ground state [35]. The $Ag_3PO_4/LaCoO_3$ nanocomposite was synthesized and presented higher visible-light catalytic degradation activity toward BPA and stability than alone Ag_3PO_4 [36]. Loading photocatalyst particles on supporter like GO/RGO, the photocatalytic activity of Ag_3PO_4 composites can also be increased. However, GO/RGO is relative expensive, which limits the practical application of the composited photocatalysts to some extent. Based on our knowledge and preliminary work, activated biochar (AC) can be used as electron conductor and photocatalyst particles supporter [37,38]. AC, as an inexpensive, non-toxic, good sorption capacity solid carbonaceous material, obtained from pyrolysis, carbonization or activation of biomass. AC can act as a supporting substrate for catalysts and provide more active sites [39]. In addition, AC has excellent electron conversion efficiency and accelerative immobilization of organic pollutants owing to graphite-like porous structure and efficiently tunable surface groups [38,40].

In this work, activated biochar (AC) was prepared from eucalyptus wood chips by phosphoric acid treatment coupled with high-temperature calcinations, the as-prepared AC act as a supporting substrate; $LaCoO_3$ nanoparticles were prepared by the sol–gel method; AC and $LaCoO_3$ were put into methanol and the suspension was sonicated, volatilized, aged, then the $LaCoO_3$/AC composite obtained. The $LaCoO_3/AC/Ag_3PO_4$ composite Z-scheme photocatalyst was formed by Ag_3PO_4 in-situ growth method with the following advantages: (1) intensifying photocatalytic activity exposed to visible-light illumination, (2) promoting the stability and the reusability. To determine the physico-chemical properties of the constructed $LaCoO_3/AC/Ag_3PO_4$ photocatalyst, the crystal phases, morphology with elemental information, functional groups, physico-chemical properties and optical properties of the photocatalyst were characterized by X-ray diffraction (XRD), transmission electron microscope (TEM), scanning electron microscope and energy dispersive X-ray spectroscopy (SEM-EDS), X-ray photoelectron spectroscopy (XPS), Fourier transform infrared (FT-IR) spectroscopy, N_2 adsorption/desorption apparatus, and UV–vis diffuse reflectance spectrophotometer (UV–vis-DRS). The photocatalytic performance of the as-prepared materials were evaluated through the degradation of BPA under visible-light irradiation, the active species in the photocatalytic process were then analyzed by trapping free radical experiment. In addition, the separation and transportation of photogenerated charges, as well as the electrochemical properties of the composites were investigated by photoluminescence spectroscopy (PL) and electrochemical impedance spectroscopy (EIS), and then based on band gap theory and test results, $LaCoO_3/AC/Ag_3PO_4$ Z-scheme photocatalytic mechanism is proposed. Finally, the main intermediate products of BPA degradation were detected by high-performance liquid chromatography-mass spectrometry (HPLC-MS) and the BPA photocatalytic degradation pathway is also inferred.

2. Material and methods

2.1. Materials

Eucalyptus wood chips were provided by Guangxi Gaofeng Farm, China. All chemical reagents are of analytical grade, obtained from local reagents supplier, and used without further purification.

2.2. Preparation of activated biochar and $LaCoO_3$ materials

The activated biocar was synthesized via phosphoric acid activation method. First, eucalyptus-wood chips (60 mesh, 10 g) were mixed with phosphoric acid (mass concentration 50%, 20 g) and keep soaked overnight. Subsequently, the obtained sample was dried, calcined at 600 °C for 2 h. Then, the obtained product was washed with deionized water to neutral, dried, grinded until passed through 80 mesh sieves and finally activated biochar obtained, labeled as AC.

The $LaCoO_3$ nanoparticles were developed by the sol–gel method based on citrate complexation according to the methods described in the literature [31]. Initially, 1.4552 g $Co(NO_3)_2{\cdot}6H_2O$ and 2.1650 g $La(NO_3)_3{\cdot}6H_2O$ were dissolved in deionized water (40 mL) by ultrasonic-assisted. Afterwards, 2.1014 g citric acid was put into and stirred for 5 h, the gel was formed at 80 °C and stirred for another 2 h. Then, the sample was freeze-dried (-50 °C) for 12 h, calcined at 700 °C for 4 h, $LaCoO_3$ was obtained.

2.3. Preparation of $LaCoO_3/BC/Ag_3PO_4$ composites

For synthesis of $LaCoO_3/AC/Ag_3PO_4$, 0.1 g of the obtained AC and 0.2 g of $LaCoO_3$ were put into 60 mL methanol and further sonicated for 30 min. The above suspension was placed at room temperature until methanol is completely volatilized, and then aged at 80 °C for 12 h, the $LaCoO_3$/AC composite obtained. Afterwards, 20 mL of 0.36 mol/L $AgNO_3$ aqueous solutions was added and kept stirred for 12 h; Ag^+ ions can be deposited on the surface of the $LaCoO_3$/AC composite sufficiently. Then, 20 mL of 0.12 mol/L $Na_2HPO_4{\cdot}12H_2O$ aqueous solutions was added dropwise to the above suspension and then kept stirred for 2 h. Finally, the formed precipitate was centrifuged, washed repeatedly using deionized water and ethanol. The collected precipitate was dried in vacuum at 60 °C for 8 h, the $LaCoO_3/AC/Ag_3PO_4$ (2:1:10) composite was obtained. The dosage of AC, $LaCoO_3$ and Ag_3PO_4 were changed, the $LaCoO_3/AC/Ag_3PO_4$ composites with different mass ratio of the constituent (2:1:15, 3:1:10) were prepared and the $LaCoO_3/Ag_3PO_4$ (2:10) composite was prepared in the same way.

2.4. Characterization

The crystal phases of the above-mentioned photocatalysts were measured by XRD (Shimadzu, Japan) with CuKα radiation ($\lambda = 0.154$ nm) at the scanning rate of 8°/min over 2θ of 10 ~ 80°. The morphology and chemical analysis of the products was observed by a SEM (ZEISS Gemini 300) and coupled with an energy dispersive X-ray spectroscopy

(EDS, OXFORD Xplore) detector. The UV–vis diffuse reflectance spectra (DRS) of the samples were obtained on a UV–vis spectrophotometer (Tianmei UV-2600). The compositions of the sample was measured and analyzed via XPS (Thermo Fisher Scientific, ESCALAB 250Xi) with Al K-Alpha (1486.8 eV) source. FT-IR (Thermo Fisher Scientific, Nicolet iS 50) was used to analyze the surface functional groups of different materials. N_2 adsorption/desorption isotherm of the samples obtained on a specific surface and porosity analyzer (Micromeritics ASAP 2460, USA). The PL spectra of the samples were obtained via on LS55 fluorescence spectrometer (Perkin-Elmer, USA) with an excitation wavelength of 485 nm. The EIS was measured on a CHI 760E electrochemical workstationn (Chen Hua, Shanghai, China).

2.5. Photocatalytic activity estimation

The photocatalytic activities of $LaCoO_3$, Ag_3PO_4, the $LaCoO_3$/Ag_3PO_4 composite and the $LaCoO_3$/AC/Ag_3PO_4 composite were estimated via photodegradation of BPA. The photocatalytic degradation of BPA was detected in a photocatalytic instrument using 500 W Xe lamp (Beijing Aulight Co. Ltd.) with a 420 nm cutoff filter. All experiments performed in the same conditions except for the different catalysts. In a typical process, 10.0 mg photocatalyst and 40 mL of 10 mg/L BPA aqueous solution was added to a quartz tube, magnetically stirred for 30 min in absence of light to achieve adsorption–desorption equilibrium and then followed by 2 h visible light illumination, approximate 1 mL of the suspension were withdrawn from the photocatalytic reactor at regular intervals and filtered immediately with syringe filters to separate the catalyst from the suspension. The BPA concentration of the filtrate was analyzed by a HPLC equipped with a solar wavelength detector (VWD) at the BPA max adsorption wavelength of 230 nm, with methanol–water (65:35, v/v) serving as the mobile phase at a flow rate of 1.0 mL min^{-1}. The C-18 column (250 × 4.6 mm) was used at25 °C with injection volume of 20 μL. The degradation efficiency of BPA was calculated by the (Eq. (1)) [40], and the BPA degradation data was fitted to the pseudo-first order kinetics model (Eq. (2)) [41].

$$\text{Degradation efficiency } (\%) = (1 - C_t/C_0) \times 100\% \quad (1)$$

$$\ln(C_t/C_0) = -k\,t \quad (2)$$

where C_0 and C_t was the BPA concentration at initial and time(t), k was the pseudo first-order rate constant. The degradation intermediates of BPA were identified by HPLC-MS (Thermo Scientific).

Furthermore, in order to find out the activate radical species in the BPA photocatalytic degradation system, three scavengers, 1 mM of 1,4-benzoquinone (DBQ), 1 mM of isopropanol (IPA) and 1 mM of disodium ethylenediaminetetraacetate (EDTA-Na_2) were used as scavengers for $^{\bullet}O_2^-$, $^{\bullet}OH$ and h^+[33,42,43], respectively. The experimental processes were similar to the photocatalytic degradation experiments.

3. Results and discussion

3.1. Characterization of photocatalysts

The XRD diagrams of $LaCoO_3$, AC, Ag_3PO_4, the $LaCoO_3$/Ag_3PO_4 (2:10) composite and the $LaCoO_3$/AC/Ag_3PO_4 (2:1:10) composite were represented in Fig. 1(a), respectively. As we can see, all of the characteristic peaks of $LaCoO_3$ were matched to rhombohedral $LaCoO_3$ (JCPDS Card No. 48-0123) [44–46] and no other impurities peaks were observed. In the curves of Ag_3PO_4, the peaks located at 20.9°, 29.7°, 33.3°, 36.6°, 47.8°, 52.6°, 55.0°, 57.2°, 71.8° were the characteristic diffraction peaks of cubic phase Ag_3PO_4 (JCPDS No.06-0505) [47–50]. With respect to the $LaCoO_3$/Ag_3PO_4 (2:10) and $LaCoO_3$/AC/Ag_3PO_4 (2:1:10) composite, the main diffraction peaks of $LaCoO_3$ and Ag_3PO_4 had no obvious changes, indicating that the crystal structure keep unchanged. However, $LaCoO_3$ diffraction peak intensity became weaker, which could be attributed to its smaller proportion in the $LaCoO_3$/Ag_3PO_4 (2:10) and $LaCoO_3$/AC/Ag_3PO_4 (2:1:10) composite. Activated biochar (AC) is an amorphous carbon with a little graphitized microcrystalline structure [51], and the low content of AC in the composite resulted in the characteristic peaks corresponding to graphitized microcrystal cannot be clearly observed in the XRD spectrum.

The FT-IR results of $LaCoO_3$/AC/Ag_3PO_4 (2:1:10), AC, $LaCoO_3$, and Ag_3PO_4 were shown in Fig. 1(b). For AC, the peak at 1639 $cm^{-1}$was corresponding to the stretching vibrations of C═O and aromatic C═C bond [52]. Additionally, the peaks at 1389, 1060, and 559 cm^{-1} were associated with the stretching vibrations of —COO [52], C—OH [53] and bending vibrations of O═P—O [54], respectively. The peaks at 594 and 554 cm^{-1} of $LaCoO_3$ were owed to the stretching vibration of the Co—O bond and the perovskite crystal structure [55]. The two peaks at 996 and 552 cm^{-1} of Ag_3PO_4 were attributed to the P—O—P symmetric stretching and the O═P—O bending vibration in PO_4^{3-}[54]. The $LaCoO_3$/AC/Ag_3PO_4 (2:1:10) composite spectrum contained peaks from Ag_3PO_4, AC and $LaCoO_3$: the peak of 558 cm^{-1} were associated with the O═P—O bending vibration [54] from Ag_3PO_4 (552 cm^{-1}, red shift) and the stretching vibration of the Co—O bond from $LaCoO_3$ (554 cm^{-1}, red shift), 1651 cm^{-1} were attributed to the stretching vibration of C═O and aromatic C═C bond from AC (1639 cm^{-1}, red shift), the broader peak appeared at 1200~–900 cm^{-1} could be caused by O—P—O [54] from Ag_3PO_4 and C—OH stretching vibration [52] from AC, respectively. The above results indicated that Ag_3PO_4 was successfully loaded on $LaCoO_3$/AC and the $LaCoO_3$/AC/Ag_3PO_4 composite formed.

The SEM, TEM images and the EDS pattern of the samples were

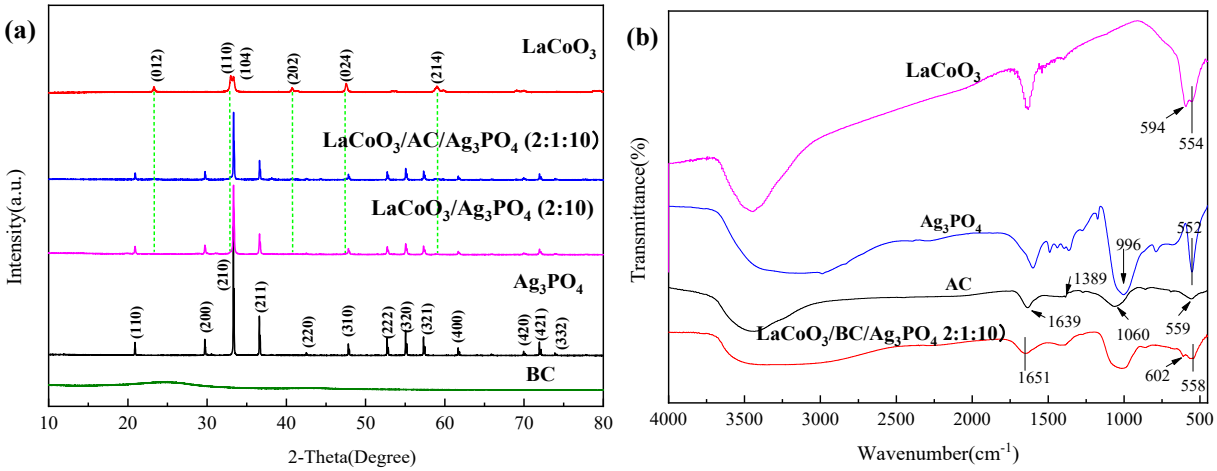

Fig. 1. (a) XRD patterns, (b) FT-IR spectra of different samples.

showed in Fig. 2. The as-prepared AC exhibited an abundant pore structure (Fig. 2 (a)), large surface area, which means there may be many active sites. The Ag_3PO_4 particles (Fig. 2 (b)) took on as an irregular spherical and agglomerated with each other, which may be due to high surface energy of single Ag_3PO_4 particles [42,47,48]. The $LaCoO_3$ sample existed plentiful irregular and agglomerate bulk particles and displayed obvious pores structure which may be formed by the staggered arrangement of particles [46] (Fig. 2 (c)). For the composite $LaCoO_3$/AC/Ag_3PO_4 (2:1:10) (Fig. 2 (d)), $LaCoO_3$/AC particles were enclosed tightly by the Ag_3PO_4, ensuring their close contact with each other. TEM was preformed to obtain the microstructure information of the composite $LaCoO_3$/AC/Ag_3PO_4 (2:1:10). As shown in Fig. 2 (e) and Fig. 2 (f), the intimate contact interface among them ensured the heterojunction was constructed through random deposition of Ag_3PO_4 particles on the $LaCoO_3$/AC substrate. It was beneficial for photogenerated electron hole pair transfers at the heterojunction.

EDS analysis was used to identify elemental composition of the $LaCoO_3$/AC/Ag_3PO_4 (2:1:10) composite (Fig. 2 (g)). From Fig. 2 (g) it was clear that the composite was composed of La, Ag, Co, P, O, and C elements. The mass percentages of Ag, La, and Co were found to be 33.20%, 3.78% and 3.78%, respectively. The mass percentages of C, O, and P were found to be 18.81%, 19.94% and 5.43%, respectively. These elements contents results also demonstrated the formation of the $LaCoO_3$/AC/Ag_3PO_4 (2:1:10) composite.

The surface chemical composition of the $LaCoO_3$/AC/Ag_3PO_4 (2:1:10) composite was characterized using XPS analysis. It was found that the composite material contained Ag 3d, P 2p, La 3d, Co 2p, O 1s and C 1s peaks (Fig. 3a), which was in agreement with the results of the EDS. The two major peaks at 367.96 eV and 373.90 eV of Ag 3d in Fig. 3b were attributed to Ag $3d_{5/2}$ and Ag $3d_{3/2}$, corresponding to the peaks of Ag^+[56]. Fig. 3c showed that the binding energy peak at 133.20 eV was associated with P^{5+} in PO_4^{3-}[42]. The binding energy peaks at around 835.30 eV, 838.50 eV, 852.15 eV and 855.20 eV in Fig. 3d were corresponding to the inner layer electrons of La $3d_{5/2}$ and La $3d_{3/2}$, proved that La existed in the form of La^{3+}[57]. In Fig. 3e, Co 2p band energy at 781.1 eV and 797.9 eV, were attributed to Co $2p_{3/2}$ and Co $2p_{1/2}$, respectively, and a typical satellite peak at 786.6 eV can be ascribed to the Co^{3+} in the hybrid [57,58]. The O 1s spectrum (Fig. 3f) displayed three peaks, the binding energy peak at 530.8 eV was consistent with O^{2-} in $LaCoO_3$ and Ag_3PO_4, while the characteristic peaks at 532.4 eV and 533.4 eV were the oxygen-containing functional groups of AC, which were associated with —OH and C═O [51]. As for C 1s spectrum in Fig. 3g was separated at four binding energies at 284.55 eV, 285.27 eV, 286.41 eV and 287.78 eV, which were attributed to C═C, C—C [28], C—OH and C═O [59], respectively. These results further confirmed the formation of the heterojunction and the co-existence of AC, Ag_3PO_4 and $LaCoO_3$ in the ternary composite, which was highly in correspondence with the XRD, FT-IR, TEM and SEM-EDS results.

The N_2 adsorption-desorptioon isotherms of the samples were presented in Fig.S1 and the corresponding BET specific surface areas (S_{BET})

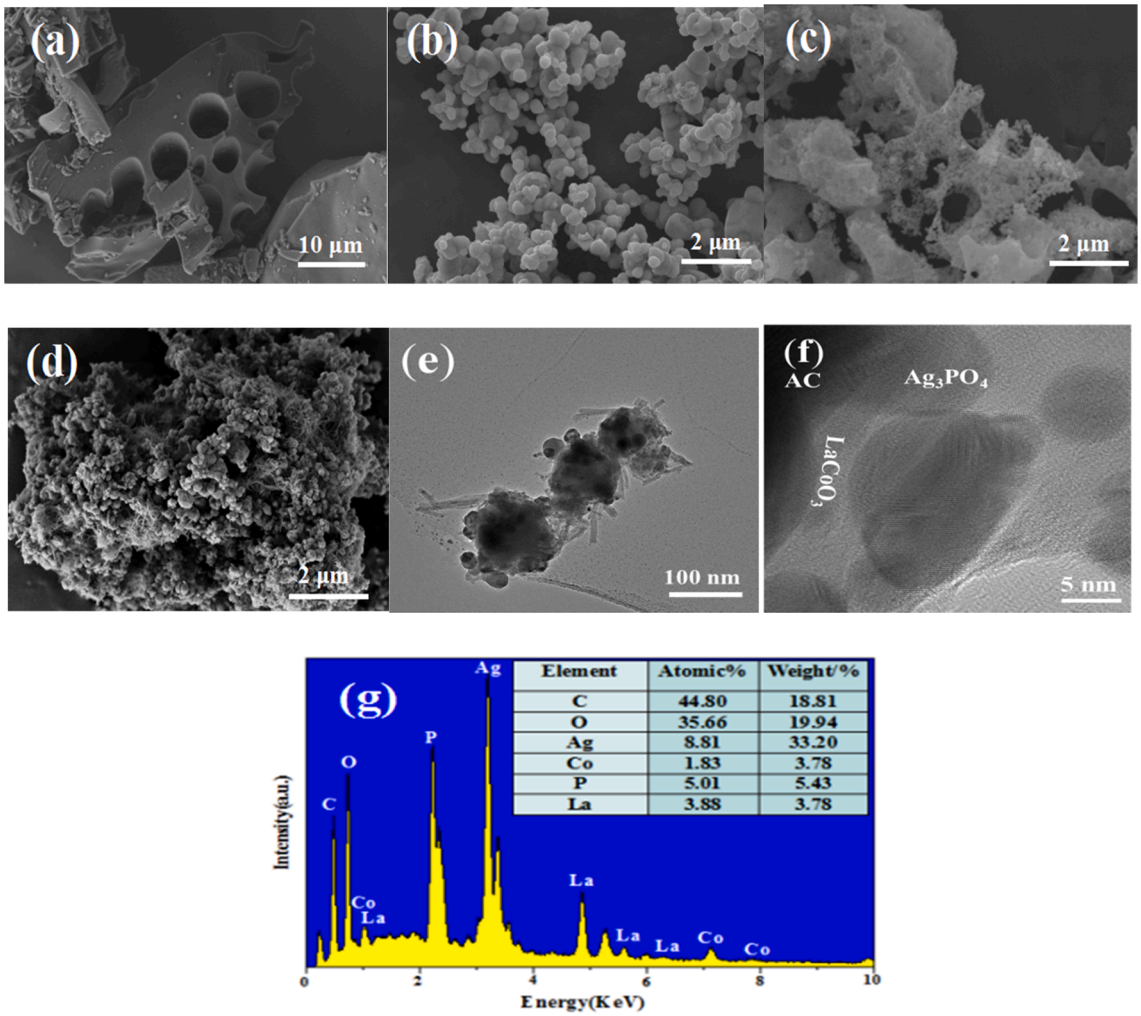

Fig. 2. SEM images of (a) AC, (b) Ag_3PO_4, (c) $LaCoO_3$;SEM(d) and TEM (e and f) of $LaCoO_3$/AC/Ag_3PO_4 (2: 1:10); (g) the EDS pattern of $LaCoO_3$/AC/Ag_3PO_4(2:1:10).

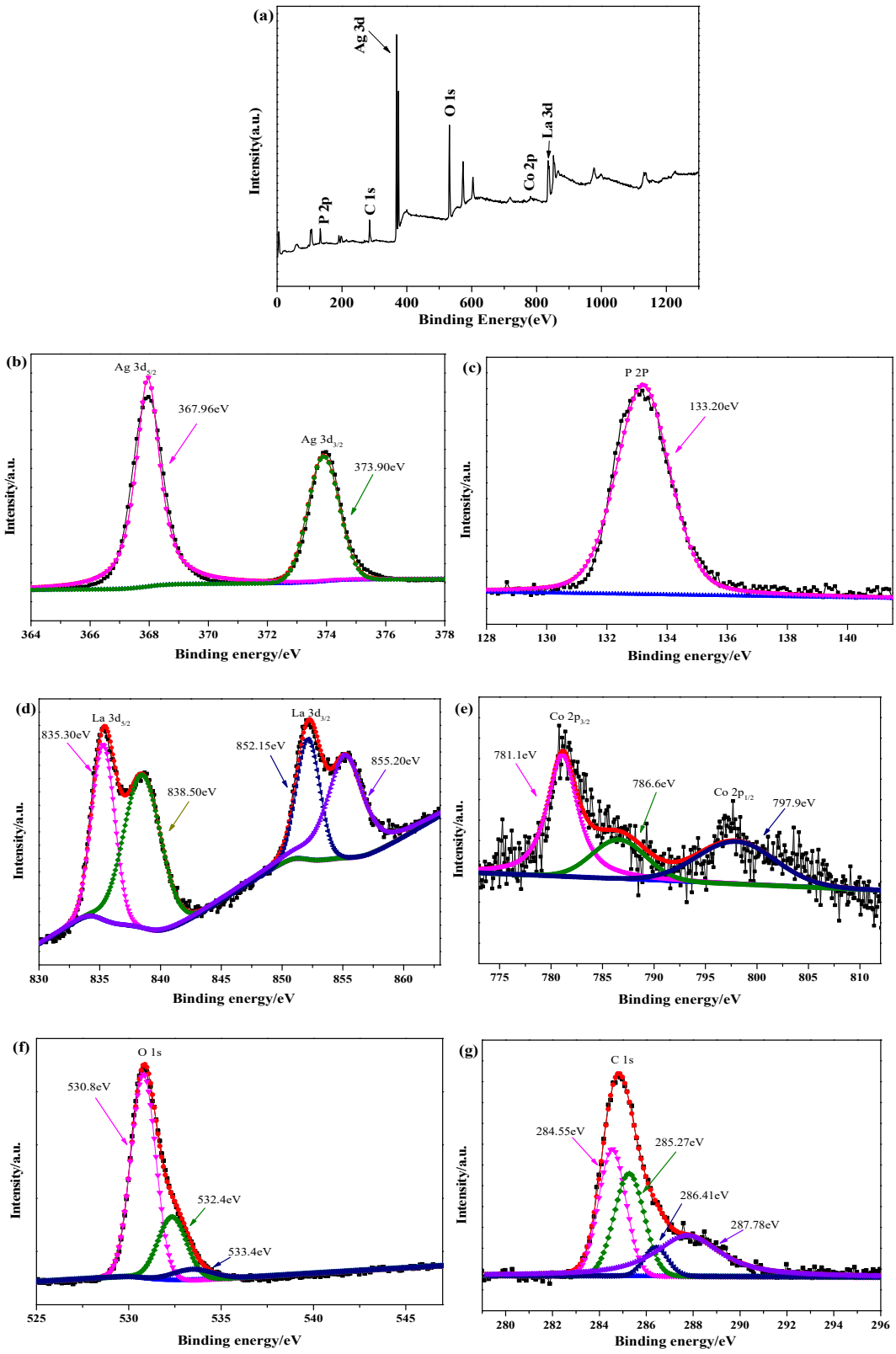

Fig. 3. XPS spectra of $LaCoO_3/AC/Ag_3PO_4$ (2:1:10) composite: (a) survey scan, (b) Ag 3d, (c) P 2p, (d) La 3d, (e) Co 2p, (f) O 1s and (g) C 1s.

and pore volume of AC, $LaCoO_3$, Ag_3PO_4, $LaCoO_3/AC/Ag_3PO_4$ (2:1:10) were showed in Table S1. Based on the IUPAC isotherm classification, the N_2 adsorption–desorption isotherms of AC, $LaCoO_3$ and $LaCoO_3/AC/Ag_3PO_4$ (2:1:10) belonged to type IV isotherms, which suggested that there were mesopore in each samples [47,60]. Ag_3PO_4 had almost no adsorption capacity. S_{BET} and pore volumes of AC, $LaCoO_3$, Ag_3PO_4, and $LaCoO_3/AC/Ag_3PO_4$ (2:1:10) were (1450.976 m^2/g, V_p 0.850 cm^3/g), (9.867 m^2/g, V_p 0.064 cm^3/g), (0.997 m^2/g, V_p 0.0018 cm^3/g), and (107.956 m^2/g, V_p 0.174 cm^3/g), respectively. Compared with alone Ag_3PO_4, S_{BET} of $LaCoO_3/AC/Ag_3PO_4$ (2:1:10) composites increased,

suggested that more active sites were exposed, and the pollutants were more easily adsorbed on the surface of $LaCoO_3/AC/Ag_3PO_4$ (2:1:10) composites, thereby photocatalytic activity was enhanced.

3.2. The photocatalytic activity

Aimed to estimate the photocatalytic activity of the samples, BPA degradation experiment had been carried out in the catalytic system. Fig. 5a displayed the degradation efficiency of BPA in no catalyst, $LaCoO_3$, Ag_3PO_4, $LaCoO_3/Ag_3PO_4$ (2:10), $LaCoO_3/AC/Ag_3PO_4$ (2:1:10), $LaCoO_3/AC/Ag_3PO_4$ (2:1:15), and $LaCoO_3/AC/Ag_3PO_4$ (3:1:10) reaction system. In presence of visible light without any photocatalyst system, BPA was scarcely degraded. Obviously in Fig. 4a, $LaCoO_3/AC/Ag_3PO_4$ had the largest adsorption capacity for BPA compared with $LaCoO_3$ and Ag_3PO_4, which was due to largest S_{BET} and pore volume of the $LaCoO_3/AC/Ag_3PO_4$ composites. Exposed to visible light illumination for 50 min, the degradation efficiency of BPA reached about 9.24 %, 36.6 % and 84.1% when the same mass of $LaCoO_3$, Ag_3PO_4 and $LaCoO_3/Ag_3PO_4$ (2:10) were added as catalyst in the reaction system, respectively. The degradation efficiency of BPA catalyzed by the $LaCoO_3/AC/Ag_3PO_4$ (2:1:10) composite was the optimal, BPA was degraded nearly 99 % after 50 min. The BPA photocatalytic degradation data were fitted using the pseudo first-order kinetic model, and the rate constants k was showed in Fig. 4b. The k catalyzed by $LaCoO_3/AC/Ag_3PO_4$ (2:1:10) ($k = 0.06528\ min^{-1}$) for BPA degradation was 10.88 times of that catalyzed by Ag_3PO_4 ($k = 0.006\ min^{-1}$), 1.56 times of that catalyzed by $LaCoO_3/Ag_3PO_4$ (2:10) ($k = 0.04191\ min^{-1}$). It suggested that the modification of Ag_3PO_4 with $LaCoO_3$ or $AC/LaCoO_3$ to construct $LaCoO_3/Ag_3PO_4$ or $LaCoO_3/AC/Ag_3PO_4$ heterojunction photocatalyst can significantly improve the photocatalytic properties of catalysts, and photocatalytic activities of $LaCoO_3/Ag_3PO_4$ was further enhanced after combination with AC. The results confirmed heterojunction photocatalyst that was Ag_3PO_4photocatalytic Ag_3PO_4 [40,51,61]

Additionally, in order to investigate the reusability of the $LaCoO_3/AC/Ag_3PO_4$ (2:1:10) composite, the reusability of Ag_3PO_4, $LaCoO_3/Ag_3PO_4$ (2:10) and $LaCoO_3/AC/Ag_3PO_4$ (2:1:10) for BPA degradation were appraised by three successive photocatalytic experimental cycles under the same conditions. The photodegradation efficiencies of $LaCoO_3/AC/Ag_3PO_4$ (2:1:10) towards BPA still reached about 64.2% after three cycles (Fig. 4c). However, the photocatalytic efficiencies of bare Ag_3PO_4 and $LaCoO_3/Ag_3PO_4$ (2:10) towards BPA were only 15.3% and 51.8% after three cycles, respectively, indicating that the photocatalytic activities and stability of $LaCoO_3/AC/Ag_3PO_4$ (2:1:10) had been improved compared with Ag_3PO_4 and $LaCoO_3/Ag_3PO_4$ (2:10). The XRD pattern of the $LaCoO_3/AC/Ag_3PO_4$ (2:1:10) composite after three cycles (Fig. 4d) showed no significant changes in the crystal phases, while the peak at 38.1° could be ascribed to the Ag^0 particles. It suggested that Ag^+ on the surface of the catalyst had been reduced to Ag^0. Ag_3PO_4 had been photocorroded and resulted in photocatalytic activities reduction [62]. However, the degree of photocorrosion and photocatalytic activities reduction of the $LaCoO_3/AC/Ag_3PO_4$ (2:1:10) composites was greatly decreased when $LaCoO_3$ and AC was introduced to Ag_3PO_4.

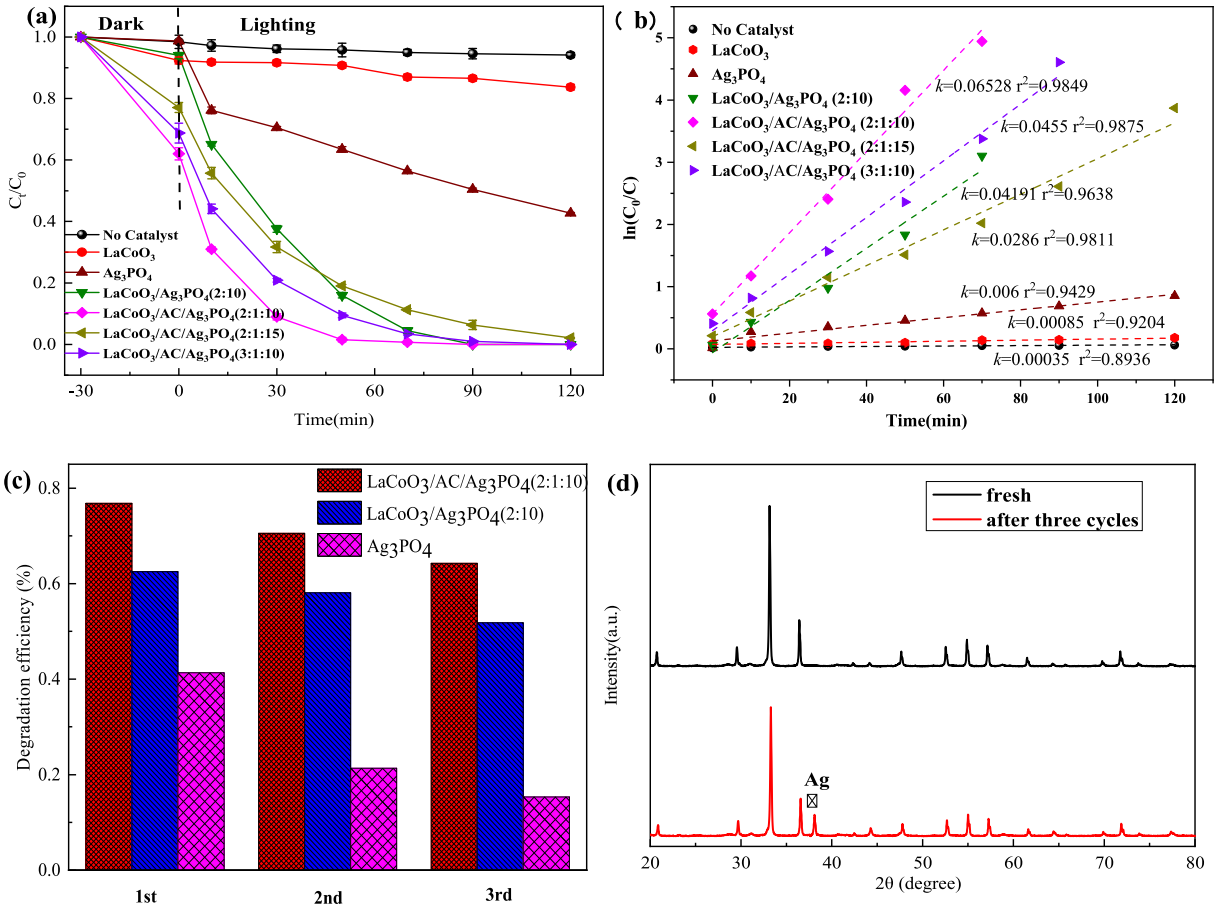

Fig. 4. (a) Effects of different catalysts on BPA photocatalytic degradation, (b) Linear simulation curve of the kinetics of BPA photocatalysis degradation by different materials, (c) Photocatalytic degradation recycle experiment of BPA, and (d) XRD patterns of $LaCoO_3/AC/Ag_3PO_4$ (2:1:10) photocatalyst before and after three cycles.

3.3. Possible mechanism of enhanced photocatalytic performance

Aimed to detect the active species produced in the photocatalytic system, an active species capture experiment was performed. EDTA-Na_2 (h^+ scavengers), DBQ ($^{\cdot}O_2^-$ scavengers) and IPA ($^{\cdot}OH$ scavengers) were used to trap h^+[29,51,55], $^{\cdot}O_2^-$[18,40,55], and $^{\cdot}OH$ [18,29,40,51,55], respectively. As depicted in Fig. 5a, when IPA and DBQ were added in the reaction system, the photodegradation efficiency of BPA decreased by 44.6% and 50.7%, respectively, while it changed little when EDTA-Na_2 added. The results suggested that $^{\cdot}OH$ and $^{\cdot}O_2^-$ were the predominant active species for BPA photodegradation catalyzed by the $LaCoO_3$/AC/Ag_3PO_4 (2:1:10) composite.

The optical absorption properties of catalysts were detected on the UV–vis diffuse reflectance spectrophotometer, and the spectra were displayed in Fig. 5b. As observed, Ag_3PO_4 exhibited an intense absorption within the visible light region with a steep band-edge at wavelength about 600 nm, higher than that reported by Chen et al [42]. $LaCoO_3$ presented a strong absorption in the entire visible light region, consistent with that reported by Yao et al [46]. AC showed a weak absorption in the visible light region, consistent with that reported by Kristy Talukdar et al [40]. After combining Ag_3PO_4 with AC and $LaCoO_3$, cut-off absorption-edge the $LaCoO_3$/AC/Ag_3PO_4 (2:1:10) composite was extended up to about 750 nm, which is beneficial for utilizing the wider visible light region. In addition, the $LaCoO_3$/AC/Ag_3PO_4 (2:1:10) composite presented obviously increase of visible light absorption in a wide response range from the visible region for Ag_3PO_4 to near-infrared region for $LaCoO_3$, and exhibited stronger visible light absorption than Ag_3PO_4. These were resulted from that the synergistic effect among $LaCoO_3$, Ag_3PO_4 and AC probably accelerated the charge transfer from Ag_3PO_4 to $LaCoO_3$ by AC, led to an obvious red shift. The formed heterostructure of $LaCoO_3$/AC/Ag_3PO_4 (2:1:10), cut-off absorption-edge was extended up to about 750 nm, which was beneficial for utilizing the wider visible light region. Moreover, $LaCoO_3$/AC/Ag_3PO_4 (2:1:10) exhibited stronger visible light absorption than Ag_3PO_4, which was

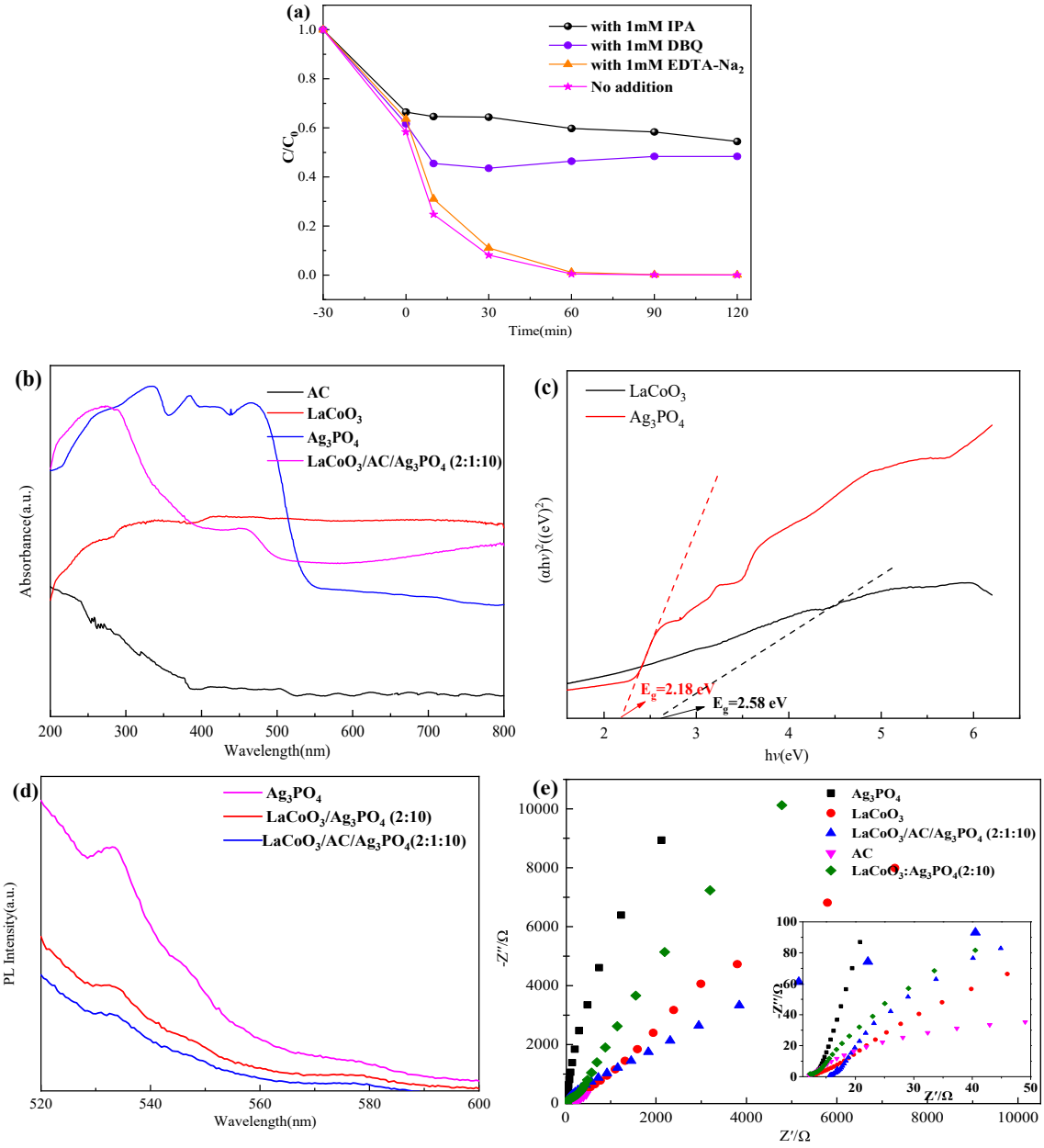

Fig. 5. (a) Effect of different radicals scavengers on the degradation efficiency of BPA in the $LaCoO_3$/AC/Ag_3PO_4 (2:1:10) reaction system, (b) UV–Vis diffusive reflectance spectra, (c) band gap energy values estimated Kubelka – Munk plots, (d) PL emission and (e) electrochemical impedance spectra of different catalysts.

helpful to enhance photocatalytic activity.

As showed in Fig. 5c, the direct band gap energy (E_g) of the photocatalysts can be calculated by the Kubelka-Munk equation (Eq. (3)) [14,32]:

$$\alpha h\nu = A(h\nu - E_g)^{1/2} \quad (3)$$

where α, ν, h and A were the absorption coefficient, light frequency, Planck's constant and a constant, respectively. The E_g of Ag_3PO_4 and $LaCoO_3$ were calculated as 2.18 and 2.58 eV in Fig. 5c, respectively. The valence band and conduction band positions of Ag_3PO_4 and $LaCoO_3$ could be calculated by formulas (4) and (5) [63]:

$$E_{CB} = \chi - E^e - 0.5E_g \quad (4)$$

$$E_{VB} = E_{CB} + E_g \quad (5)$$

where E_{VB} and E_{CB} represented the valence band and conduction band edge potentials of the semiconductors, respectively, and χ was absolute electronegativity. The χ values of Ag_3PO_4 and $LaCoO_3$ were about 5.97 eV [64] and 5.64 eV [33], respectively. E^e was the energy of free electrons with the hydrogen scale (about 4.5 eV vs normal hydrogen electrode (NHE)). Based on the above calculation, the conduction band potential of Ag_3PO_4 and $LaCoO_3$ were 0.38 eV and − 0.15 eV, and the valence band potential were 2.56 eV and 2.43 eV, respectively.

In general, the separation, migration and recombination processes of photogenerated charge carriers of the heterostructure materials can be evaluated by photoluminescence (PL) spectra measurements. As shown in Fig. 5d, the Ag_3PO_4 sample had highest fluorescence intensity centered at around 530 nm due to the recombination of the photogenerated electrons and holes [50]. The stronger the fluorescence intensity was, the faster the recombination rate between photogenerated electron-hole pairs, the shorter the lifetime of photogenerated charge carriers [65]. However, the $LaCoO_3$/AC/Ag_3PO_4 (2:1:10) composite showed a decrease in the PL intensities compared to the pure Ag_3PO_4 and $LaCoO_3$/Ag_3PO_4 (2:10) samples, implying that the synergistic effects between the $LaCoO_3$/AC and Ag_3PO_4 help to successfully prohibit the recombination of charge carriers, and there were higher separation efficiency between photogenerated electron-hole pairs in the $LaCoO_3$/AC/Ag_3PO_4 (2:1:10) ternary systems.

Moreover, EIS measurement was also conducted to further investigate the photoelectrochemical properties of the photocatalyst. It was generally believed that the diameter of the semicircle on the EIS Nyquist diagram corresponded to charge transfer resistance, and the smaller arc radius represented an improved charge carrier migration, lower charge transfer resistance and higher charge transfer efficiency in a semiconductor material [66]. As depicted in Fig. 5e, $LaCoO_3$/AC/Ag_3PO_4 (2:1:10) showed smaller arc radius, corresponding to lower resistance than that of $LaCoO_3$/Ag_3PO_4 (2:10) and Ag_3PO_4. According to the above photocatalytic property evaluation results, it can be concluded that the $LaCoO_3$/AC/Ag_3PO_4 (2:1:10) composite possessed the optimum e^-–h^+pairs separation and transfer efficiency.

According to the above results, the mechanism of BPA photodegradation catalyzed by the $LaCoO_3$/AC/Ag_3PO_4 (2:1:10) composites could be proposed and illustrated in Fig. 6. Under visible light irradiation, the electron-hole pairs (e^-–h^+) of Ag_3PO_4 and $LaCoO_3$ could be excited by high-energy photons. Then, e^- on the valence band (VB) migrated to the conduction band (CB), while h^+ remained on the respective VB. The e^- on the CB of Ag_3PO_4 were not combined with h^+ on the VB immediately but transferred to the VB of $LaCoO_3$ through mediator and recombined with h^+ at the VB of $LaCoO_3$; that is, AC, served as e^- transfer mediator, can help photogenerated e^- on the CB of Ag_3PO_4 transfer to the VB of $LaCoO_3$. There are mainly two reasons: First, the VB of $LaCoO_3$ is lower than that of Ag_3PO_4, making its e^- drop path shorter; secondly, a heterojunction is formed between $LaCoO_3$ and Ag_3PO_4 owing to AC served as mediator; AC served as e^- transfer mediator, which leads to the easier transfer of e^- from the CB of Ag_3PO_4

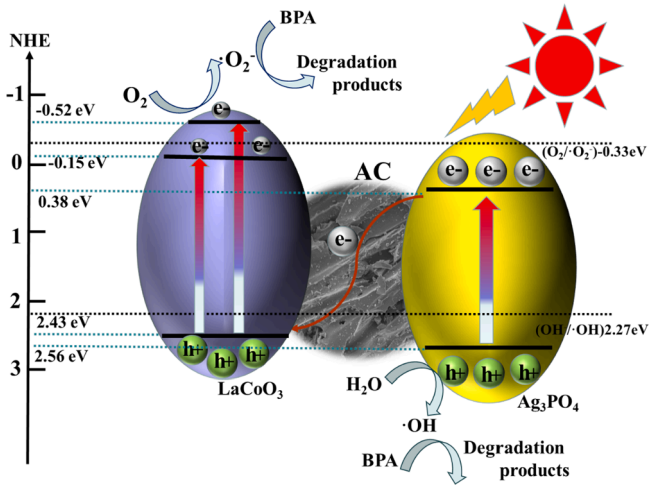

Fig. 6. Schematic diagram of degradation of BPA by $LaCoO_3$/AC/Ag_3PO_4 (2:1:10) under visible light irradiation.

to the VB of $LaCoO_3$, on the VB of $LaCoO_3$, e^- from the CB of Ag_3PO_4 are continuously obtained, and then recombined with h^+ at the VB of $LaCoO_3$, and e^- on the VB of $LaCoO_3$ migrated to the CB the $LaCoO_3$. In a word, the VB potential of $LaCoO_3$ was less negative than the CB potential of Ag_3PO_4, the photogenerated e^- from the CB of Ag_3PO_4 can migrate rapidly through AC to the VB of $LaCoO_3$ and combined with h^+ of $LaCoO_3$. Consequently, the photogenerated e^- in the CB of Ag_3PO_4 and h^+ in the VB of $LaCoO_3$ were efficiently separated. The E_{VB} of both $LaCoO_3$ and Ag_3PO_4 were more positive than OH^-/$^{\cdot}OH$ (2.27 eV vs NHE) [67], the h^+ left on the VB of Ag_3PO_4 can oxidize OH^- from H_2O into $^{\cdot}OH$. Since the E_{CB} (−0.15 eV) of $LaCoO_3$ was less negative than $O_2/^{\cdot}O_2^-$ (−0.33 eV vs NHE) [68,69], it seems that the electrons in the CB of $LaCoO_3$ cannot react with oxygen in water to form $^{\cdot}O_2^-$. However, according to the formula: $\lambda = 1240/E_g$ (E_g is the energy bandgap) [69–72], the highest electronic energy level of $LaCoO_3$ can reach − 0.52 eV when the excitation wavelength is less than 449 nm. In other words, under visible light (λ = 449–420 nm) irradiation, the e^- on the VB of $LaCoO_3$ could be excited up to a more negative potential edge position (−0.52 eV ~ −0.33 eV) [68,69,71,73]. In this case, the reformed high-level-energy electrons in CB of $LaCoO_3$ had more negative potential than the standard redox potential of $O_2/^{\cdot}O_2^-$ (−0.33 eV vs NHE) [68,69,71,73], and $^{\cdot}O_2^-$ can be generated. Therefore, $^{\cdot}OH$ and $^{\cdot}O_2^-$ play a major role in the degradation of BPA by $LaCoO_3$/AC/Ag_3PO_4 (2:1:10), which was consistent with the free radical capture experiment. Therefore, the Z-scheme heterojunction photocatalytic system was formed, and the Z-scheme mechanism was highly consistent with the free radical capture experiments results.

3.4. Degradation pathway of BPA

In order to speculate the possible degradation pathway of BPA, the main degradation intermediate products were detected by HPLC-MS and were listed in Fig.S2. Based on degradation intermediates analysis results, the potential BPA degradation pathways catalyzed by the $LaCoO_3$/AC/Ag_3PO_4 (2:1:10) composites under visible light illumination were summarized in Fig. 7, including hydroxylation, oxidation, ketonization and cyclic cleavage [41,74,75]. One degradation pathway was that the hydroxylation of BPA took place, which could cause the formation of hydroxylated BPA, and then further degraded to 4-isopropanol *o*-phenol and *p*-phenol. In addition, another degradation pathway was the broken of the C-C bond in BPA to form *p*-phenol and 4-isopropyl phenol, which was then further oxidized to *p*-benzoquinone and 2-phenylpropionic acid. After further oxidation and ring opening, the aromatic molecules could be converted into H_2O and CO_2 eventually.

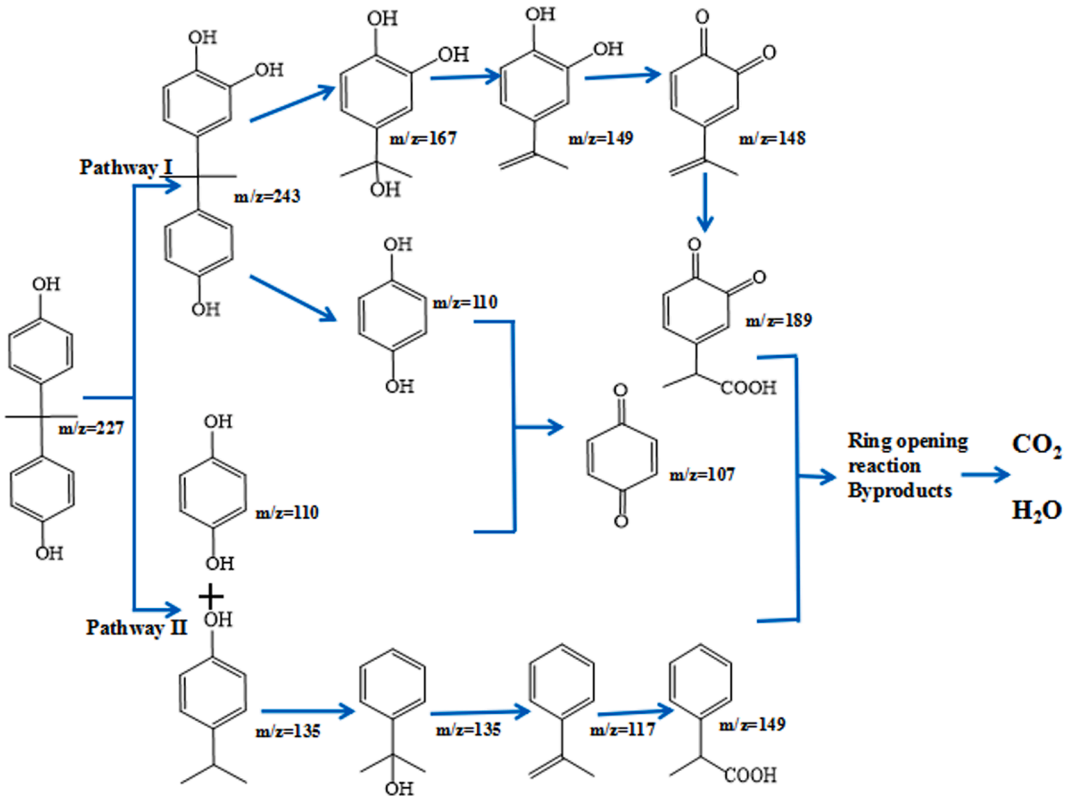

Fig. 7. Proposedpathways of BPA photodegradation.

4. Conclusion

In this work, the $LaCoO_3/AC/Ag_3PO_4$ composites were successfully synthesized by a facile in-situ growth method, which exhibited excellent potential for BPA degradation under visible light irradiation compared with Ag_3PO_4 and $LaCoO_3/Ag_3PO_4$. At the same time, AC, acted as the adsorption center and electron conductor in photocatalyst, provided a use for waste biomass. Through the cycle experiment, it was proved that the reusability and stability of the $LaCoO_3/AC/Ag_3PO_4$ (2:1:10) composite was much higher than that of alone Ag_3PO_4 and $LaCoO_3/Ag_3PO_4$ (2:10). The dominant active radical species were $^{\bullet}OH$ and $^{\bullet}O_2^-$ based on the active species capture experiments results. Furthermore, the photodegradation process of BPA involved hydroxylation, oxidation, ketonization and cyclic cleavage according to the degradation intermediates of BPA analyzed by HPLC-MS. Z-scheme $LaCoO_3$/activated carbon(AC)/Ag_3PO_4 can be considered as an efficient photocatalyst and its practical applications in the removal of endocrine disrupting chemical is prospective.

CRediT authorship contribution statement

Xinyan Bu: Conceptualization, Methodology, Investigation, Validation, Formal analysis, Data curation, Writing – original draft. **Congjin Chen:** Conceptualization, Methodology, Investigation, Validation, Formal analysis, Data curation, Resources, Writing – review & editing, Supervision, Project administration, Funding acquisition. **Xilian Zhao:** Investigation, Validation, Formal analysis, Writing – review & editing. **Quanlong Huang:** Investigation, Formal analysis. **Xiufen Liao:** Formal analysis, Validation. **Hui Fan:** Investigation. **Peiwen Wang:** . **Huayu Hu:** Resources, Supervision. **Yanjuan Zhang:** Resources, Supervision. **Zuqiang Huang:** Resources, Supervision.

Declaration of Competing Interest

The authors declare that they have no known competing financial interests or personal relationships that could have appeared to influence the work reported in this paper.

Acknowledgment

This work was supported by the National Natural Science Foundation of China (31660183), the Dean/Opening Project of Guangxi Key Laboratory of Petrochemical Resource Processing and Process Intensification Technology (2020K003).

Appendix A. Supplementary material

Supplementary data to this article can be found online at https://doi.org/10.1016/j.apsusc.2022.152887.

References

[1] S. Rodriguez-Mozaz, S. Chamorro, E. Marti, B. Huerta, M. Gros, A. Sànchez-Melsió, C.M. Borrego, D. Barceló, J.L. Balcázar, Occurrence of antibiotics and antibiotic resistance genes in hospital and urban wastewaters and their impact on the receiving river, Water Res. 69 (2015) 234–242.

[2] A.A. Horton, A. Walton, D.J. Spurgeon, E. Lahive, C. Svendsen, Microplastics in freshwater and terrestrial environments: Evaluating the current understanding to identify the knowledge gaps and future research priorities, Sci. Total Environ. 586 (2017) 127–141.

[3] Y. Deng, L. Tang, G. Zeng, Z. Zhu, M. Yan, Y. Zhou, J. Wang, Y. Liu, J. Wang, Insight into highly efficient simultaneous photocatalytic removal of Cr(VI) and 2,4-diclorophenol under visible light irradiation by phosphorus doped porous ultrathin g-C_3N_4 nanosheets from aqueous media: Performance and reaction mechanism, Appl. Catal. B 203 (2017) 343–354.

[4] C. Zhou, C. Lai, D. Huang, G. Zeng, C. Zhang, M. Cheng, L. Hu, J. Wan, W. Xiong, M. Wen, X. Wen, L. Qin, Highly porous carbon nitride by supramolecular preassembly of monomers for photocatalytic removal of sulfamethazine under visible light driven, Appl. Catal. B 220 (2018) 202–210.

[5] H. Che, G. Che, H. Dong, W. Hu, H. Hu, C. Liu, C. Li, Fabrication of Z-scheme Bi_3O_4Cl/g-C_3N_4 2D/2D heterojunctions with enhanced interfacial charge

separation and photocatalytic degradation various organic pollutants activity, Appl. Surf. Sci. 455 (2018) 705–716.
[6] Y.Q. Huang, C.K.C. Wong, J.S. Zheng, H. Bouwman, R. Barra, B. Wahlström, L. Neretin, M.H. Wong, Bisphenol A (BPA) in China: A review of sources, environmental levels, and potential human health impacts, Environ. Int. 42 (2012) 91–99.
[7] H. Zhang, Y. He, L. Lai, G. Yao, B.o. Lai, Catalytic ozonation of Bisphenol A in aqueous solution by Fe3O4–MnO2 magnetic composites: Performance, transformation pathways and mechanism, Sep. Purif. Technol. 245 (2020) 116449, https://doi.org/10.1016/j.seppur.2019.116449.
[8] S. Zhang, S. Song, P. Gu, R. Ma, D. Wei, G. Zhao, T. Wen, R. Jehan, B. Hu, X. Wang, Visible-light-driven activation of persulfate over cyano and hydroxyl group co-modified mesoporous g-C_3N_4 for boosting bisphenol A degradation, J. Mater. Chem. A 7 (10) (2019) 5552–5560.
[9] Y. Fu, P. Xu, D. Huang, G. Zeng, C. Lai, L. Qin, B. Li, J. He, H. Yi, M. Cheng, C. Zhang, Au nanoparticles decorated on activated coke via a facile preparation for efficient catalytic reduction of nitrophenols and azo dyes, Appl. Surf. Sci. 473 (2019) 578–588.
[10] C. Lai, M. Zhang, B. Li, D. Huang, G. Zeng, L. Qin, X. Liu, H. Yi, M. Cheng, L. Li, Z. Chen, L. Chen, Fabrication of CuS/BiVO4 (0 4 0) binary heterojunction photocatalysts with enhanced photocatalytic activity for Ciprofloxacin degradation and mechanism insight, Chem. Eng. J. 358 (2019) 891–902.
[11] B. Li, C. Lai, G. Zeng, L. Qin, H. Yi, D. Huang, C. Zhou, X. Liu, M. Cheng, P. Xu, C. Zhang, F. Huang, S. Liu, Facile Hydrothermal Synthesis of Z-Scheme $Bi_2Fe_4O_9$/Bi_2WO_6 Heterojunction Photocatalyst with Enhanced Visible Light Photocatalytic Activity, ACS Appl. Mater. Inter. 10 (22) (2018) 18824–18836.
[12] W. Xue, X. Hu, E. Liu, J. Fan, Novel reduced graphene oxide-supported $Cd_{0.5}Zn_{0.5}S$/g-C_3N_4 Z-scheme heterojunction photocatalyst for enhanced hydrogen evolution, Appl. Surf. Sci. 447 (2018) 783–794.
[13] C. Li, D. Zhu, S. Cheng, Y. Zuo, Y. Wang, C. Ma, H. Dong, Recent research progress of bimetallic phosphides-based nanomaterials as cocatalyst for photocatalytic hydrogen evolution, Chinese Chem. Lett. (2021), https://doi.org/10.1016/j.cclet.2021.07.057.
[14] H. Dong, Y. Zuo, N. Song, S. Hong, M. Xiao, D. Zhu, J. Sun, G. Chen, C. Li, Bimetallic synergetic regulating effect on electronic structure in cobalt/vanadium co-doped carbon nitride for boosting photocatalytic performance, Appl. Catal. B 287 (2021) 119954.
[15] M. Mousavi, A. Habibi-Yangjeh, M. Abitorabi, Fabrication of novel magnetically separable nanocomposites using graphitic carbon nitride, silver phosphate and silver chloride and their applications in photocatalytic removal of different pollutants using visible-light irradiation, J. Colloid Interf. Sci. 480 (2016) 218–231.
[16] X. Xie, C. Mao, X. Liu, L. Tan, Z. Cui, X. Yang, S. Zhu, Z. Li, X. Yuan, Y. Zheng, K.W. K. Yeung, P.K. Chu, S. Wu, Tuning the Bandgap of Photo-Sensitive Polydopamine/Ag_3PO_4/Graphene Oxide Coating for Rapid, Noninvasive Disinfection of Implants, ACS Central Sci. 4 (6) (2018) 724–738.
[17] D. Li, H. Wang, H. Tang, X. Yang, Q. Liu, Remarkable Enhancement in Solar Oxygen Evolution from $MoSe_2$/Ag_3PO_4 Heterojunction Photocatalyst via In Situ Constructing Interfacial Contact, ACS Sustain. Chem. Eng. 7 (9) (2019) 8466–8474.
[18] B. Shao, X. Liu, Z. Liu, G. Zeng, Q. Liang, C. Liang, Y. Cheng, W. Zhang, Y. Liu, S. Gong, A novel double Z-scheme photocatalyst Ag_3PO_4/Bi_2S_3/Bi_2O_3 with enhanced visible-light photocatalytic performance for antibiotic degradation, Chem. Eng. J. 368 (2019) 730–745.
[19] Y. Bi, S. Ouyang, N. Umezawa, J. Cao, J. Ye, Facet Effect of Single-Crystalline Ag_3PO_4 Sub-microcrystals on Photocatalytic Properties, J. Am. Chem. Soc. 133 (17) (2011) 6490–6492.
[20] L. Liu, J. Liu, D.D. Sun, Graphene oxide enwrapped Ag_3PO_4 composite: towards a highly efficient and stable visible-light-induced photocatalyst for water purification, Catal. Sci. Technol. 2 (2012) 2525.
[21] A. Wu, C. Tian, W. Chang, Y.u. Hong, Q.i. Zhang, Y. Qu, H. Fu, Morphology-controlled synthesis of Ag_3PO_4 nano/microcrystals and their antibacterial properties, Mater. Res. Bull. 48 (9) (2013) 3043–3048.
[22] Y. Lin, S. Wu, C. Yang, M. Chen, X. Li, Preparation of size-controlled silver phosphate catalysts and their enhanced photocatalysis performance via synergetic effect with MWCNTs and PANI, Appl. Catal. B 245 (2019) 71–86.
[23] C. Liu, J. Xu, J. Niu, M. Chen, Y. Zhou, Direct Z-scheme Ag_3PO_4/$Bi_4Ti_3O_{12}$ heterojunction with enhanced photocatalytic performance for sulfamethoxazole degradation, Sep. Purif. Technol. 241 (2020) 116622, https://doi.org/10.1016/j.seppur.2020.116622.
[24] S. Chen, D. Huang, G. Zeng, W. Xue, L. Lei, P. Xu, R. Deng, J. Li, M. Cheng, In-situ synthesis of facet-dependent $BiVO_4$/Ag_3PO_4/PANI photocatalyst with enhanced visible-light-induced photocatalytic degradation performance: Synergism of interfacial coupling and hole-transfer, Chem. Eng. J. 382 (2020) 122840.
[25] J. Jin, M. Liu, L. Feng, H. Wang, Y. Wang, T.A.H. Nguyen, Y. Wang, J. Lu, Y. Li, M. Bao, 3D Bombax-structured carbon nanotube sponge coupling with Ag_3PO_4 for tetracycline degradation under ultrasound and visible light irradiation, Sci. Total Environ. 695 (2019) 133694, https://doi.org/10.1016/j.scitotenv.2019.133694.
[26] N. Shao, Z. Hou, H. Zhu, J. Wang, C.P. François-Xavier, Novel 3D core-shell structured CQDs/Ag_3PO_4@Benzoxazine tetrapods for enhancement of visible-light photocatalytic activity and anti-photocorrosion, Appl. Catal. B 232 (2018) 574–586.
[27] K.e. Ouyang, N. Jiang, W. Xue, S. Xie, Enhanced photocatalytic activities of visible light-responsive Ag_3PO_4-GO photocatalysts for oxytetracycline hydrochloride degradation, Colloids Surf., A 604 (2020) 125312, https://doi.org/10.1016/j.colsurfa.2020.125312.
[28] W. Shi, F. Guo, S. Yuan, In situ synthesis of Z-scheme Ag_3PO_4/$CuBi_2O_4$ photocatalysts and enhanced photocatalytic performance for the degradation of tetracycline under visible light irradiation, Appl. Catal. B 209 (2017) 720–728.
[29] L. Liu, L. Ding, Y. Liu, W. An, S. Lin, Y. Liang, W. Cui, A stable Ag3PO4@PANI core@shell hybrid: Enrichment photocatalytic degradation with π-π conjugation, Appl. Catal. B 201 (2017) 92–104.
[30] X. Liu, W. Chen, H. Jiang, Facile synthesis of Ag/Ag_3PO_4 AMB composite with improved photocatalytic performance, Chem. Eng. J. 308 (2017) 889–896.
[31] S. Yao, R. Zheng, R. Li, Y. Chen, X. Zhou, X. Ning, L. Zhan, J. Luo, $LaCoO_3$ acts as a high-efficiency co-catalyst for enhancing visible-light-driven tetracycline degradation of BiOI, J. Am. Ceram. Soc. 103 (3) (2020) 1709–1721.
[32] R. Wang, C. Ye, H. Wang, F. Jiang, Z-Scheme $LaCoO_3$/g-C_3N_4 for Efficient Full-Spectrum Light-Simulated Solar Photocatalytic Hydrogen Generation, ACS Omega 5 (47) (2020) 30373–30382.
[33] Z. Jin, R. Hu, H. Wang, J. Hu, T. Ren, One-step impregnation method to prepare direct Z-scheme $LaCoO_3$/g-C_3N_4 heterojunction photocatalysts for phenol degradation under visible light, Appl. Surf. Sci. 491 (2019) 432–442.
[34] H. Chen, G. Wei, X. Liang, P. Liu, H. He, Y. Xi, J. Zhu, The distinct effects of substitution and deposition of Ag in perovskite $LaCoO_3$ on the thermally catalytic oxidation of toluene, Appl. Surf. Sci. 489 (2019) 905–912.
[35] C.-L. Ma, J. Cang, First principles investigation on the band gap of the ground state of, Solid State Commun. 150 (41-42) (2010) 1983–1986.
[36] J. Guo, Y.-Z. Dai, X.-J. Chen, L.-l. Zhou, T.-H. Liu, Synthesis and characterization of Ag_3PO_4/$LaCoO_3$ nanocomposite with superior mineralization potential for bisphenol A degradation under visible light, J. Alloy. Compd. 696 (2017) 226–233.
[37] Q. Huang, C. Chen, X. Zhao, X. Bu, X. Liao, H. Fan, W. Gao, H. Hu, Y. Zhang, Z. Huang, Malachite green degradation by persulfate activation with $CuFe_2O_4$@ biochar composite: Efficiency, stability and mechanism, J. Environ. Chem. Eng. 9 (4) (2021) 105800, https://doi.org/10.1016/j.jece:2021.105800.
[38] H. Wang, Z. Ye, C. Liu, J. Li, M. Zhou, Q. Guan, P. Lv, P. Huo, Y. Yan, Visible light driven Ag/Ag_3PO_4/AC photocatalyst with highly enhanced photodegradation of tetracycline antibiotics, Appl. Surf. Sci. 353 (2015) 391–399.
[39] K. Sun, Q. Huang, M. Ali, Y. Chi, J. Yan, Producing Aromatic-Enriched Oil from Mixed Plastics Using Activated Biochar as Catalyst, ENERG. FUEL. 32 (4) (2018) 5471–5479.
[40] K. Talukdar, B.-M. Jun, Y. Yoon, Y. Kim, A. Fayyaz, C.M. Park, Novel Z-scheme Ag3PO4/Fe3O4-activated biochar photocatalyst with enhanced visible-light catalytic performance toward degradation of bisphenol A, J. Hazard. Mater. 398 (2020) 123025, https://doi.org/10.1016/j.jhazmat.2020.123025.
[41] R.S. Sahu, Y.-H. Shih, W.-L. Chen, New insights of metal free 2D graphitic carbon nitride for photocatalytic degradation of bisphenol A, J. Hazard. Mater. 402 (2021) 123509, https://doi.org/10.1016/j.jhazmat.2020.123509.
[42] X. Chen, C. Yu, R. Zhu, N. Li, J. Chen, Q. Lin, S. Xu, X. Chen, H. Wang, Photocatalytic performance and mechanism of Z-Scheme $CuBi_2O_4$/Ag_3PO_4 in the degradation of diclofenac sodium under visible light irradiation: Effects of pH, H_2O_2, and $S_2O_8^{2-}$, Sci. Total Environ. 711 (2020) 134643, https://doi.org/10.1016/j.scitotenv.2019.134643.
[43] D. Zhu, Q. Zhou, Nitrogen doped g-C3N4 with the extremely narrow band gap for excellent photocatalytic activities under visible light, Appl. Catal. B 281 (2021) 119474.
[44] Y. Zhang, Q. Li, Y. Long, J. Zou, Z. Song, C. Liu, L. Liu, F. Qi, B. Xu, Z. Chen, Catalytic ozonation benefit from the enhancement of electron transfer by the coupling of g-C_3N_4 and $LaCoO_3$: Discussion on catalyst fabrication and electron transfer pathway, Appl. Catal. B 254 (2019) 569–579.
[45] Y. Luo, J. Zuo, X. Feng, Q. Qian, Y. Zheng, D. Lin, B. Huang, Q. Chen, Good interaction between well dispersed Pt and $LaCoO_3$ nanorods achieved rapid Co3+/Co2+ redox cycle for total propane oxidation, Chem. Eng. J. 357 (2019) 395–403.
[46] S. Yao, J. Wu, W. Li, R. Zheng, R. Li, Y. Chen, J. Luo, X. Zhou, $LaCoO_3$ co-catalyst modified Ag_2CrO_4 for improved visible-light-driven photocatalytic degradation of tetracycline, Sep. Purif. Technol. 227 (2019) 115691, https://doi.org/10.1016/j.seppur.2019.115691.
[47] B. Borjigin, L. Ding, H. Li, X. Wang, A solar light-induced photo-thermal catalytic decontamination of gaseous benzene by using Ag/Ag_3PO_4/CeO_2 heterojunction, Chem. Eng. J. 402 (2020) 126070, https://doi.org/10.1016/j.cej.2020.126070.
[48] Y. Ma, J. Li, Y. Jin, K. Gao, H. Cai, G. Ou, The enhancement mechanism of ultra-active Ag3PO4 modified by tungsten and the effective degradation towards phenolic pollutants, Chemosphere 285 (2021) 131440, https://doi.org/10.1016/j.chemosphere.2021.131440.
[49] Y. Song, H. Zhao, Z. Chen, W. Wang, L. Huang, H. Xu, H. Li, The CeO 2/Ag 3 PO 4 photocatalyst with stability and high photocatalytic activity under visible light irradiation : CeO 2/Ag 3 PO 4 photocatalyst with stability and high photocatalytic activity, Phys. Status Solidi A 213 (9) (2016) 2356–2363.
[50] D.J. Martin, G. Liu, S.J. Moniz, Y. Bi, A.M. Beale, J. Ye, J. Tang, Efficient visible driven photocatalyst, silver phosphate: performance, understanding and perspective, Chem. Soc. Rev. 44 (2015) 7808–7828.
[51] Y. Zhai, Y. Dai, J. Guo, L. Zhou, M. Chen, H. Yang, L. Peng, Novel biochar@$CoFe_2O_4$/Ag_3PO_4 photocatalysts for highly efficient degradation of bisphenol a under visible-light irradiation, J. Colloid Interf. Sci. 560 (2020) 111–121.
[52] M.G. Gonçalves, P.A. da Silva Veiga, M.R. Fornari, P. Peralta-Zamora, A. S. Mangrich, S. Silvestri, Relationship of the physicochemical properties of novel ZnO/biochar composites to their efficiencies in the degradation of sulfamethoxazole and methyl orange, Sci. Total Environ. 748 (2020) 141381, https://doi.org/10.1016/j.scitotenv.2020.141381.
[53] I. Moulefera, F.J. García-Mateos, A. Benyoucef, J.M. Rosas, J. Rodríguez-Mirasol, T. Cordero, Effect of Co-solution of Carbon Precursor and Activating Agent on the

Textural Properties of Highly Porous Activated Carbon Obtained by Chemical Activation of Lignin With H_3PO_4, Front. Mater. 7 (2020).
[54] G. Hou, Y. Li, W. An, S. Gao, W. Zhang, W. Cui, Fabrication and photocatalytic activity of floating type Ag_3PO_4/$ZnFe_2O4$/FACs photocatalyst, Mater. Res. Bull. 94 (2017) 263–271.
[55] J. Guo, P. Li, Z. Yang, A novel Z-scheme g- C_3N_4/$LaCoO_3$ heterojunction with enhanced photocatalytic activity in degradation of tetracycline hydrochloride, Catal. Commun. 122 (2019) 63–67.
[56] X. Li, H. Hu, L. Xu, C. Cui, D. Qian, S. Li, W. Zhu, P. Wang, P. Lin, J. Pan, C. Li, Z-schematic water splitting by the synergistic effect of a type-II heterostructure and a highly efficient oxygen evolution catalyst, Appl. Surf. Sci. 441 (2018) 61–68.
[57] X. Li, H. Gao, Influence of Ce doping on catalytic oxidation of NO on $LaCoO_3$ (011) surface: A DFT study, Appl. Surf. Sci. 499 (2020) 143866, https://doi.org/10.1016/j.apsusc.2019.143866.
[58] J. Ge, Y. Cui, Y. Cai, J. Qian, L. Liu, F. Meng, F. Wang, 2D organic-α-$Co(OH)_2$ material and derived Co/C composites with bifunctions of anti-corrosion and microwave absorption, Compos. B Eng. 224 (2021) 109172.
[59] X. Chen, Y. Dai, J. Guo, T. Liu, X. Wang, Novel Magnetically Separable Reduced Graphene Oxide (RGO)/$ZnFe_2O_4$/Ag_3PO_4 Nanocomposites for Enhanced Photocatalytic Performance toward 2,4-Dichlorophenol under Visible Light, Ind. Eng. Chem. Res. 55 (3) (2016) 568–578.
[60] X. Li, Z. Zeng, G. Zeng, D. Wang, R. Xiao, Y. Wang, C. Zhou, H. Yi, S. Ye, Y. Yang, W. Xiong, A "bottle-around-ship" like method synthesized yolk-shell Ag_3PO_4@MIL-53(Fe) Z-scheme photocatalysts for enhanced tetracycline removal, J. Colloid Interf. Sci. 561 (2020) 501–511.
[61] J. Shi, J. Wang, L. Liang, Z. Xu, Y.u. Chen, S. Chen, M. Xu, X. Wang, S. Wang, Carbothermal synthesis of biochar-supported metallic silver for enhanced photocatalytic removal of methylene blue and antimicrobial efficacy, J. Hazard. Mater. 401 (2021) 123382, https://doi.org/10.1016/j.jhazmat.2020.123382.
[62] H. Shi, S. Yang, C. Han, Z. Niu, H. Li, X. Huang, J. Ma, Fabrication of Ag/Ag_3PO_4/WO_3 ternary nanoparticles as superior photocatalyst for phenol degradation under visible light irradiation, Solid State Sci. 96 (2019) 105967, https://doi.org/10.1016/j.solidstatesciences.2019.105967.
[63] Y. Shaveisi, S. Sharifnia, E. Karamian, Application of mixture experimental design for photocatalytic ammonia degradation by sunlight-driven WO_3-Ag_3PO_4-ZnO ternary photocatalysts, Int. J. Energ. Res. 43 (9) (2019) 4879–4897.
[64] X. Guan, L. Guo, Cocatalytic Effect of $SrTiO_3$ on Ag_3PO_4 toward Enhanced Photocatalytic Water Oxidation, ACS Catal. 4 (9) (2014) 3020–3026.
[65] Z. Bian, Y. Feng, H. Li, J. Zhan, Fabrication of Ag_3PO_4/TiO_2@molecular sieve (MS) ternary composites with remarkably enhanced visible light-responded photocatalytic activity and mechanism insight, Environ. Res. 190 (2020) 109984, https://doi.org/10.1016/j.envres.2020.109984.
[66] Y.-X. Li, X. Wang, C.-C. Wang, H. Fu, Y. Liu, P. Wang, C. Zhao, S-TiO_2/UiO-66-NH_2 composite for boosted photocatalytic Cr(VI) reduction and bisphenol A degradation under LED visible light, J. Hazard. Mater. 399 (2020) 123085, https://doi.org/10.1016/j.jhazmat.2020.123085.
[67] Q. Liu, J. Shen, X. Yang, T. Zhang, H. Tang, 3D reduced graphene oxide aerogel-mediated Z-scheme photocatalytic system for highly efficient solar-driven water oxidation and removal of antibiotics, Appl. Catal. B 232 (2018) 562–573.
[68] T. Li, H. Wei, H. Jia, T. Xia, X. Guo, T. Wang, L. Zhu, Mechanisms for Highly Efficient Mineralization of Bisphenol A by Heterostructured Ag_2WO_4/Ag_3PO_4 under Simulated Solar Light, ACS Sustain. Chem. Eng. 7 (4) (2019) 4177–4185.
[69] J. Cao, B. Xu, H. Lin, B. Luo, S. Chen, Chemical etching preparation of BiOI/BiOBr heterostructures with enhanced photocatalytic properties for organic dye removal, Chem. Eng. J. 185-186 (2012) 91–99.
[70] M. Xie, X. Fu, L. Jing, P. Luan, Y. Feng, H. Fu, Long-Lived, Visible-Light-Excited Charge Carriers of TiO_2/$BiVO_4$ Nanocomposites and their Unexpected Photoactivity for Water Splitting, Adv. Energy Mater. 4 (5) (2014) 1300995, https://doi.org/10.1002/aenm.201300995.
[71] C. Wang, P. Du, L. Luo, Y. Tian, W. Li, Utilizing Upconversion Emission to Improve the Photocatalytic Performance of the BiOI Microplate: A Bifunctional Platform for Pollutant Degradation and Hydrogen Production, Ind. Eng. Chem. Res. 60 (2021) 16245–16257.
[72] N. Raeisi-Kheirabadi, A. Nezamzadeh-Ejhieh, A Z-scheme g-C_3N_4/Ag_3PO_4 nanocomposite: Its photocatalytic activity and capability for water splitting, Int. J. Hydrogen Energ. 45 (2020) 33381–33395.
[73] C. Chang, L. Zhu, S. Wang, X. Chu, L. Yue, Novel Mesoporous Graphite Carbon Nitride/BiOI Heterojunction for Enhancing Photocatalytic Performance Under Visible-Light Irradiation, ACS Appl. Mater. Inter. 6 (7) (2014) 5083–5093.
[74] B. Guo, T. Xu, L. Zhang, S. Li, A heterogeneous fenton-like system with green iron nanoparticles for the removal of bisphenol A: Performance, kinetics and transformation mechanism, J. Environ. Manage. 272 (2020) 111047.
[75] T. Ahamad, M. Naushad, Y. Alzaharani, S.M. Alshehri, Photocatalytic degradation of bisphenol-A with g-C_3N_4/MoS_2-PANI nanocomposite: Kinetics, main active species, intermediates and pathways, J. Mol. Liq. 311 (2020) 113339.